Theoretical Reinvestigation of the O(3 P) + C 6 H 6 Reaction: Quantum Chemical and Statistical Rate Calculations †

ARTICLE *in* THE JOURNAL OF PHYSICAL CHEMISTRY A · JUNE 2007

Impact Factor: 2.69 · DOI: 10.1021/jp0660886 · Source: PubMed

3 AUTHORS, INCLUDING:

Thanh Lam Nguyen
University of Texas at Austin
72 PUBLICATIONS **1,377** CITATIONS

SEE PROFILE

Jozef Peeters
University of Leuven
205 PUBLICATIONS **4,431** CITATIONS

SEE PROFILE

Theoretical Reinvestigation of the $O(^3P) + C_6H_6$ Reaction: Quantum Chemical and Statistical Rate Calculations†

Thanh Lam Nguyen, Jozef Peeters, and Luc Vereecken*

Department of Chemistry, University of Leuven, Celestijnenlaan 200F, B-3001, Leuven, Belgium

Received: September 18, 2006; In Final Form: November 17, 2006

The lowest-lying triplet and singlet potential energy surfaces for the $O(^3P) + C_6H_6$ reaction were theoretically characterized using the "complete basis set" CBS-QB3 model chemistry. The primary product distributions for the multistate multiwell reactions on the individual surfaces were then determined by RRKM statistical rate theory and weak-collision master equation analysis using the exact stochastic simulation method. It is newly found that electrophilic O-addition onto a carbon atom in benzene can occur in parallel on two triplet surfaces, $^3A'$ and $^3A''$; the results predict O-addition to be dominant up to combustion temperatures. Major expected end-products of the addition routes include phenoxy radical + H•, phenol and/or benzene oxide/oxepin, in agreement with the experimental evidence. While c-C_6H_5O• + H• are nearly exclusively formed via a spin-conservation mechanism on the lowest-lying triplet surface, phenol and/or benzene oxide/oxepin are mainly generated from the lowest-lying singlet surface after inter-system crossing from the initial triplet surface. CO + c-C_5H_6 are predicted to be minor products in flame conditions, with a yield ≤ 5%. The O + $C_6H_6 \rightarrow$ c-C_5H_5• + •CHO channel is found to be unimportant under all relevant combustion conditions, in contrast with previous theoretical conclusions (*J. Phys. Chem. A* **2001**, *105,* 4316). Efficient H-abstraction pathways are newly identified, occurring on two different electronic state surfaces, $^3B_1$ and $^3B_2$, resulting in hydroxyl plus phenyl radicals; they are predicted to play an important role at higher temperatures in hydrocarbon combustion, with estimated contributions of ca. 50% at 2000 K. The overall thermal rate coefficient k(O + C_6H_6) at 300−800 K was computed using multistate transition state theory: $k(T) = 3.7 \times 10^{-16} \times T^{1.66} \times \exp(-1830\ \mathrm{K}/T)$ cm^3 molecule^{-1} s^{-1}, in good agreement with the experimental data available.

I. Introduction

Benzene is recognized as a key intermediate in almost all hydrocarbon flames,[1,2] playing an important role as the "first aromatic ring" in the formation of polycyclic aromatic hydrocarbons (PAHs) and soot. It is hypothesized to be formed mainly by a combination of two propargyl radicals,[3,4] or by degradation of higher aromatics[5] if present in the fuel such as in current gasolines to increase the octane rating.[6] Under fuel-lean to moderately fuel-rich combustion conditions, one of the major benzene consumption pathways is its reaction with triplet ground state oxygen atoms.[4,5,7−10] Therefore, elucidating the reaction mechanism and predicting the product branching ratios of the elementary C_6H_6 + O reaction over wide temperature and pressure ranges is of key importance to our understanding of the overall reaction mechanisms of hydrocarbon flames as well as to the optimization of combustion processes.

The reaction of benzene with triplet O atom can in principle result in various primary products, presented in Table 1 with their experimental reaction enthalpies, when available.[11] With the exception of the direct H-abstraction channel 3, all these channels proceed via electrophilic O-addition onto a C atom forming an initial triplet, vibrationally excited, biradical adduct (triplet oxybenzene). While the spin-conserving reaction channels 1, 2, and 3 occur on a triplet electronic state surface, the remaining channels 4−9 occur via a spin-forbidden mechanism, involving intersystem crossing (ISC) of the initial triplet oxybenzene to either singlet phenol or singlet benzene oxide. These "hot" intermediates, possessing high internal energies by chemical activation, are either deactivated by multiple collisions with the bath gas or isomerize to other singlet isomers and/or decompose to various products on the singlet electronic state surface.

Reaction channel 1, producing phenoxy plus hydrogen radicals, was first detected in the crossed molecular beam experiments by Lee and co-workers[12] and recently confirmed in the multicollision work by Fontijn et al.,[13] while recent theoretical calculations carried out at the high CBS-QB3 level of theory also supported phenoxy + H formation.[14] Both the experimental[12,13] and theoretical[14] work showed this channel to be major. Although there is no experimental evidence yet for reaction channel 2 forming c-C_5H_5• + •CHO, earlier theoretical calculations predicted that this channel could be important at high temperatures.[14] Reaction channel 3, producing phenyl plus hydroxyl radicals via direct H-abstraction, is endoergic by ca. 12 kcal/mol. Therefore, at $T \leq 1300$ K, it cannot compete with the exothermal O−addition/elimination mechanisms.[15] However, OH radical production was detected in a crossed molecular beam experiment at high collisional energies of 16.5 kcal/mol.[16] This product channel was theoretically predicted to play an important role at higher temperatures ($T \geq 1500$ K).[17]

The product of singlet phenol arising from the reaction channel 4 is well established.[12,18−21] Phenol was even found under collision-free conditions in crossed molecular beam experiments,[12,21] due to the very long lifetime of the nascent,

† Part of the special issue "James A. Miller Festschrift".

* Corresponding author. E-mail: Luc.Vereecken@chem.kuleuven.be. Fax: int-32-16-327992.

10.1021/jp0660886 CCC: $37.00
Published on Web 01/25/2007

TABLE 1: Calculated Reaction Enthalpies (kcal/mol) at 0 K (ΔH^0_r) for Various Reaction Channels in the $O(^3P) + C_6H_6$ Reaction Using the CBS-QB3 Level of Theory, Where Experimental Enthalpies Reduced to 0 K Are Also Listed When Available[11]

reaction channels	ΔH^0_r	experiment[a]
$O(^3P) + c\text{-}C_6H_6 \rightarrow c\text{-}C_6H_5O^\bullet + H^\bullet$ (1)	−15.8	-14.6 ± 3
$O(^3P) + c\text{-}C_6H_6 \rightarrow c\text{-}C_5H_5^\bullet + {}^\bullet CHO$ (2)	−7.3	-6.5 ± 2
$O(^3P) + c\text{-}C_6H_6 \rightarrow c\text{-}C_6H_5^\bullet + {}^\bullet OH$ (3)	12.2	10.2 ± 2
$O(^3P) + c\text{-}C_6H_6 \rightarrow$ phenol (4)	−101.5	-101.9 ± 1
$O(^3P) + c\text{-}C_6H_6 \rightarrow c\text{-}C_5H_6 + CO$ (5)	−73.7	-74.0 ± 1
$O(^3P) + c\text{-}C_6H_6 \rightarrow c\text{-}C_6H_4 + H_2O$ (6)	−28.0	-30.8 ± 4
$O(^3P) + c\text{-}C_6H_6 \rightarrow$ benzene oxide/oxepin (7)	−56.6/−57.2	
$O(^3P) + c\text{-}C_6H_6 \rightarrow$ 2,4-/2,5-cyclohexadienone (8)	−82.5/−84.0	
$O(^3P) + c\text{-}C_6H_6 \rightarrow$ butadienyl ketene (9)	−54.2	

[a] Mainly taken from ref 11; all values were obtained at 0 K: $\Delta H^0_f(O) = 58.98$ kcal/mol; $\Delta H^0_f(H) = 51.63$ kcal/mol; $\Delta H^0_f(CO) = -27.2$ kcal/mol; $\Delta H^0_f(OH) = 8.84$ kcal/mol; $\Delta H^0_f(HCO) = 9.95$ kcal/mol; $\Delta H^0_f(H_2O) = -57.10$ kcal/mol; $\Delta H^0_f(c\text{-}C_5H_6) = 36.19$ kcal/mol; $\Delta H^0_f(c\text{-}C_6H_6) = 24.0$ kcal/mol; $\Delta H^0_f(c\text{-}C_6H_5) = 84.3$ kcal/mol; $\Delta H^0_f(c\text{-}C_6H_5OH) = -18.93 \pm 1$ kcal/mol, derived from $\Delta H^{298}_f(c\text{-}C_6H_5OH) = -23.03$ kcal/mol and ΔE(thermal correction-TC) = 4.1 kcal/mol computed at the CBS-QB3 level; $\Delta H^0_f(c\text{-}C_5H_5) = 67 \pm 2$ kcal/mol, derived from $\Delta H^{298}_f(c\text{-}C_5H_5) = 63.5 \pm 1$ kcal/mol[73] and ΔE(TC) = 3.5 kcal/mol; $\Delta H^0_f(o\text{-}C_6H_4) = 109.3 \pm 4$ kcal/mol, derived from $\Delta H^{298}_f(c\text{-}C_6H_4) = 105.9 \pm 3.3$ kcal/mol[74] and ΔE(TC) = 3.4 kcal/mol; $\Delta H^0_f(c\text{-}C_6H_5O) = 16.8 \pm 3$ kcal/mol, derived from $\Delta H^{298}_f(c\text{-}C_6H_5O) = 12.9 \pm 1.5$ kcal/mol[75] and ΔE(TC) = 3.9 kcal/mol.

chemically activated singlet intermediates.[12] The production of CO, via reaction channel 5, is a subject of some controversy. Earlier, Sloane[21] observed CO as a major product in his crossed molecular beam experiment. In contrast with this finding, Lee and co-workers[12] observed CO as a very minor product in a similar experiment, but at higher collision energies. In two recent multicollision experiments, the yield of CO, if produced, was estimated to be less than 5%.[13,22] The production of H_2O, from the reaction channel 6, has not been reported so far. Other singlet products such as benzene oxide, cyclohexadienone, and butadienyl ketene arising from the channels 7−9, have recently been detected in the $\lambda \geq 280$ nm photolysis of benzene/ozone mixtures in an argon matrix at 12 K,[23] where ozone photolysis was assumed to lead to triplet ground state O atoms.

Thermal rate coefficients for the $O(^3P) + C_6H_6$ reaction have been measured over a wide temperature range ($298\ K \leq T < 1500\ K$).[15,22,24−29] From these data, the Arrhenius activation energy was derived to be about 4−5 kcal/mol; at room temperature, a rate coefficient of $(1.7 \pm 0.3) \times 10^{-14}$ cm^3 molecule^{-1} s^{-1} is recommended.[30]

There are two published theoretical studies relevant to the title reaction. Barckholtz et al.[17] characterized the O-addition and H-abstraction channels using the B3LYP/6-311+G(d,p)//B3LYP/6-31G(d) level of theory; additionally, these authors computed thermal rate coefficients using conventional transition state theory.[17] Unfortunately, their computed B3LYP barrier height of 0.2 kcal/mol[17] is significantly lower than the experimental Arrhenius activation energy of 4−5 kcal/mol. Subsequent decomposition and/or isomerization steps of the initial oxybenzene adduct were not considered. Hodgson et al.[14] characterized the triplet $^3A''$ electronic state surface using the high-level CBS-QB3 theory, supplemented by RRKM calculations. Neither the H-abstraction channel, the triplet $^3A'$, nor the singlet electronic state surface and its crossing seams with the triplet surfaces were investigated.

As seen above, the $O(^3P) + C_6H_6$ reaction mechanism appears to be rather complicated, comprising among others multistep isomerization/decomposition processes and also nonradiative transitions from triplet to singlet electronic state surfaces. In addition, the yields of the various primary products are likely to be very sensitive to temperature and pressure. It is worth noting that in the various kinetic modeling studies of the oxidation of benzene by O different reaction channels were adopted as dominant; some authors[31,32] assumed that the title reaction mainly occurs via the channels 1 and 3, while others[33,34] considered the channels 3 and 4 as predominant.

Therefore, high-level quantum chemical calculations on all relevant reaction surfaces, in combination with state-of-the-art statistical kinetic analyses over wide temperature and pressure ranges, appear to be in order for elucidating the detailed mechanisms and predicting the product distributions of the fundamental and important $O + C_6H_6$ reaction.

II. Methodology

II.1. Quantum Chemical Calculations. Geometries of stationary points on the triplet and singlet surfaces were optimized at the hybrid density functional B3LYP/6-311G(d,p) level of theory,[35,36] followed by analytical frequency calculations at the same level to verify the stationary points located (one imaginary frequency for a transition structure and all positive frequencies for a minimum). Intrinsic reaction coordinate (IRC)[37,38] calculations were also performed at this level to establish the correct connections between the reaction intermediates; all IRC calculations are shown in Figures S14 and S20−S57 in the Supporting Information. To obtain more accurate relative energies, the complete basis set model chemistry CBS-QB3[39] was used.

For some stationary points, e.g., the singlet biradicals **S1**, **S1ex**, and **S10**, whose wave function possesses a multireference character or near-degeneracy effects, we used the CASSCF-(8,8)/cc-pVDZ level of theory[40,41] to reoptimize geometries. Energies were subsequently refined employing the CASPT2-(8,8)/cc-pVDZ level[42] based on the CASSCF reference wave function, thereby taking dynamic electron correlations into account.

To investigate the proximity or possible overlap of the triplet and singlet potential energy surfaces at or near the geometry of the initial triplet oxybenzene adduct, and so to explore possible nonradiative transitions to singlet phenol or benzene oxide (see further), we employed the CASPT2(8,8)/cc-pVDZ level based on the CASSCF reference wave function to compute single-point energies at each point along IRC(triplet UB3LYP) optimized geometries.

The DFT-B3LYP and CBS-QB3 calculations were performed using the Gaussian 03 package,[43] while the CASSCF and CASPT2 calculations used the Dalton[44] and Molpro[45] packages; all optimized stationary-point geometries, energies, harmonic vibration frequencies, and rotational constants are given in the

Supporting Information. To simplify the notation for stationary points, in this paper **T**, **S**, and **TS** stand for a triplet minimum, singlet minimum, and transition structure, respectively.

II.2. RRKM/Master Equation Calculations. Product distributions as a function of temperature and pressure ($P = 10^{-4}-10^{5}$ Torr, $T = 300-2000$ K) for the $O(^3P) + C_6H_6$ reaction proceeding on the triplet and singlet surfaces-considered as being adiabatic-were separately obtained by solution of the weak-collision master equation using Gillespie's exact stochastic simulation method,[46-48] explained in detail in our earlier paper[49] and discussed briefly here. In the energy-grained master equation, the ceiling energy considered was 200 kcal/mol above the initial triplet oxybenzene adduct **T1** and a small energy band size of 0.03 kcal/mol (10 cm^{-1}) was chosen to ensure that the density of states does not change significantly within the band. To obtain the product distribution with high statistical precision, a large number of stochastic trials of $\sim 10^7$ were used. In this application, the Mersenne Twister (MT19937)[50] random number generator was used.

The Lennard-Jones collision parameters for bath gas Ar are $\sigma = 3.47$ Å and $\epsilon/k_B = 114$ K.[51] Since no collision parameters for $[C_6H_6O]$ are available in the literature, the values $\sigma = 5.92$ Å and $\epsilon/k_B = 410$ K were estimated based on those of toluene $C_6H_5CH_3$.[51] Thus, the collision frequency $Z_{LJ}[M]$ was estimated at $\sim 1.1 \times 10^{10}$ s^{-1} at 1 atm and room temperature. The probability density function for collisional energy transfer was computed using the biexponential model of Troe.[52] An average energy transferred per collision $\langle \Delta E \rangle_{all}$ of -200 cm^{-1} was adopted. The initial vibrational energy distribution $F_v(E)$ of formation of the triplet $^{\bullet}C_6H_6O^{\bullet}$ adduct **T1** from $O(^3P) + C_6H_6$ via **TS1** was derived in the usual way from detailed balance considerations.[53] A "sink" was used to collect intermediates stabilized by deactivating collisions with the bath gas; the cutoff energy is located at 8 kcal/mol below the lowest-lying decomposition transition structure. The fraction of intermediates collected in these sinks will assume thermal energy distributions through collisions with the bath gas; their subsequent fate in unimolecular or bimolecular reactions depends on the reaction conditions and can be accommodated in chemical kinetic modeling studies.

The statistical RRKM theory[53-58] of unimolecular reaction rates is used to compute the energy-specific rate constants $k(E)$ for a reactant with an internal energy E:

$$k(E) = \frac{\alpha}{h} \times \frac{G^{\neq}(E - E^{\neq})}{\rho(E)} \qquad (10)$$

where α is the reaction pathway degeneracy, h is Planck's constant, $E^{\neq}$ is the barrier height for the reaction, $G^{\neq}(E - E^{\neq})$ is the sum of vibrational states of the transition state (TS) for energies from 0 up to $E - E^{\neq}$, and $\rho(E)$ is the density of states for a reactant molecule with internal energy E. The Beyer-Swinehart-Stein-Rabinovitch algorithm[59,60] was used to calculate the sum and density of states in eq 10, employing a grain size of 0.003 kcal/mol (1 cm^{-1}).

III. Results and Discussion

III.1. Potential Energy Surfaces. According to the spin-conservation rule, the reaction of triplet O atom with benzene can initially proceed on the triplet electronic state surface via either electrophilic O-addition onto a C atom or by direct H-abstraction, as discussed separately below. All the various reaction pathways on these initial triplet electronic state surfaces (PES) are depicted in Scheme 1; the relative energies of the main, rate-determining reaction routes effectively determining the reaction product distribution on the triplet PES are presented in Figure 1. Unless mentioned otherwise, the CBS-QB3 energy values will be used in the following discussions; they are in good agreement with the available experimental data (see Table 1) with discrepancies of about 1-2 kcal/mol. Optimized geometries for all key stationary points on the triplet PES are shown in Figure 2.

SCHEME 1: Various Reaction Pathways for the O + C_6H_6 Reaction on Triplet PES, Where Bold Arrows Indicate Dominant Reaction Routes

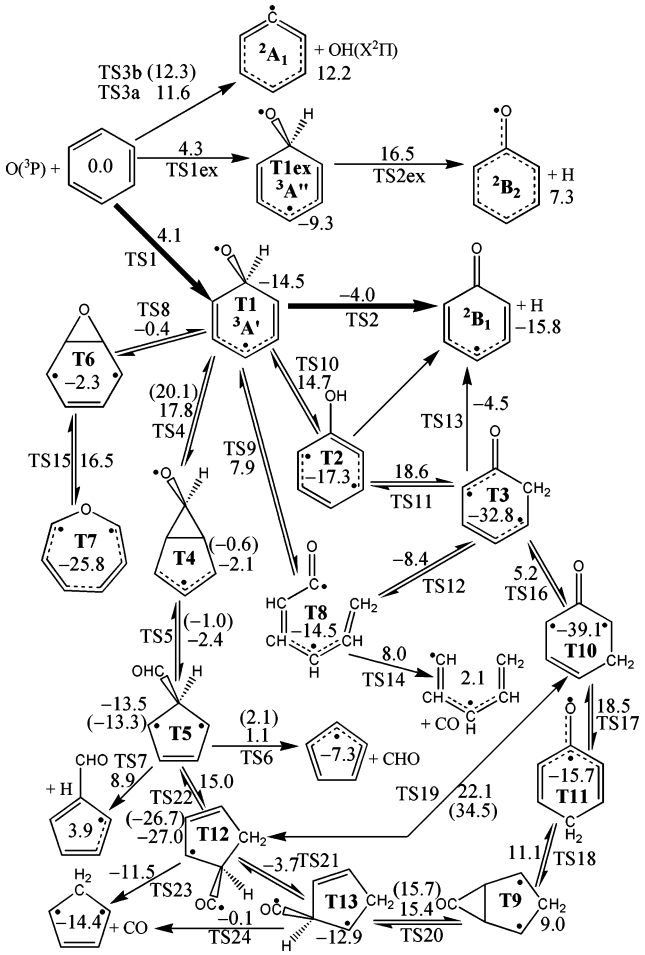

Figure 1. Energy diagram of the most important routes for the O + C_6H_6 reaction on triplet PES, as computed at the CBS-QB3 level of theory.

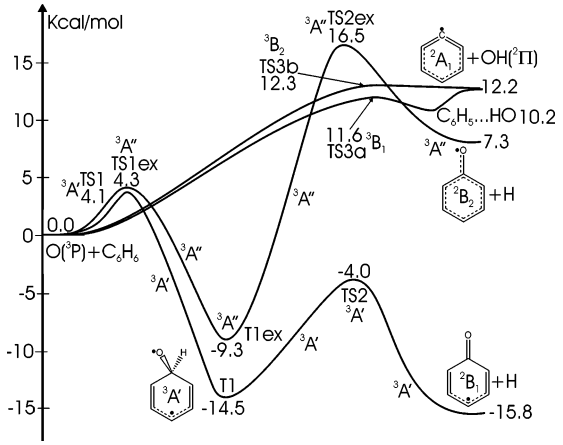

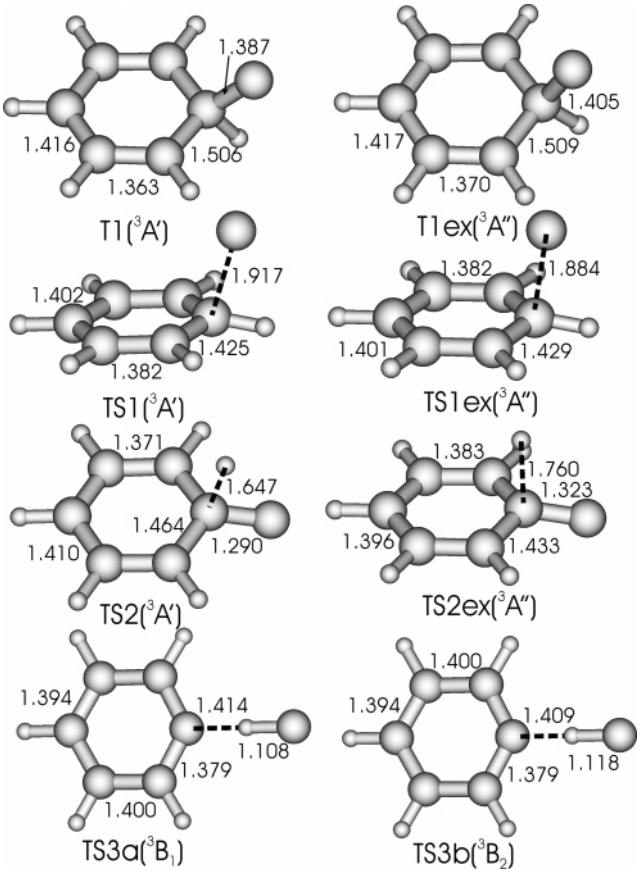

Figure 2. B3LYP-optimized geometries for some key stationary points on triplet PES.

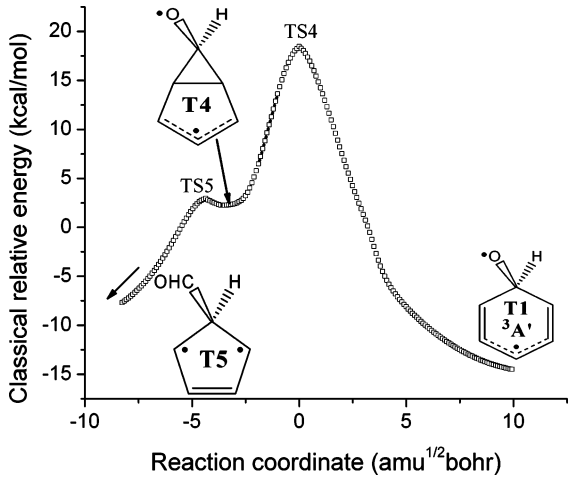

Figure 3. IRC(B3LYP/6-311G(d,p)) calculations for the **T1** → **TS4** → **T4** → **TS5** → **T5** route.

to the vibrationally excited •C_6H_6O• triplet biradical adduct, followed by its decomposition and/or isomerization on the triplet PES, was already theoretically characterized at the CBS-QB3 level by Hodgson et al.[14] Interestingly, although we used the same level of theory as Hodgson et al.,[14] our results show important differences, significantly affecting the reaction mechanism. First, our CBS-QB3 total energy for benzene, calculated using both Gaussian 98 and Gaussian 03, is about 0.6 kcal/mol above the value computed by Hodgson et al.[14] using Gaussian 98; the reason for this difference is unclear. Second, and more importantly, the ^{3}A″ electronic state triplet biradical •C_6H_6O• adduct—denoted as **T1ex** in this work—was characterized by Hodgson et al.[14] as the lowest-energy initial triplet adduct and, failing an IRC analysis, erroneously assumed to connect directly to the other triplet isomers and to the main products phenoxy + H, all in their ground states. However, we newly identified another electronic state, ^{3}A′, of triplet •C_6H_6O•, denoted here as **T1**, as the true ground state, 5.2 kcal/mol lower in energy than **T1ex**. Our IRC calculations show that both **T1** and **T1ex** connect directly with the initial reactants O + C_6H_6, via **TS1** and **TS1ex**, respectively (see Figures S14 and S15 in the Supporting Information). Analogous O-onto-carbon addition mechanisms in parallel on ^{3}A′ and ^{3}A″ electronic state surfaces have been characterized earlier for the reactions of O atoms with C_2H_2,[61] C_2H_4,[62] and C_3H_4.[63] As a result, for the case at hand, reaction pathways on the lowest-lying triplet PES rather start from the triplet ^{3}A′ •C_6H_6O• ground-state adduct **T1** instead of the excited ^{3}A″ **T1ex** state of Hodgson et al.[14] Third, Hodgson et al.[14] suggested the O(^{3}P) + C_6H_6 → **TS1ex** → ^{3}[•C_6H_6O•] **T1ex** → **TS3** → ^{3}[C_6H_5CHO] → **TS10** → c-C_6H_5 + CHO route (see Figure 4 in ref 14) to be significant at higher temperatures as, according to their work, the ^{3}[•C_6H_6O•] → **TS3** → ^{3}[C_6H_5-CHO] step faces a barrier height of 7 kcal/mol, only 1.6 kcal/mol higher than the ^{3}[•C_6H_6O•] → **TS2** → c-C_6H_5O• + H• step (see Figure 4 in ref 14). In contrast, our IRC calculations (see Figure 3) show that the ^{3}[•C_6H_6O•] **T1** → ^{3}[C_6H_5CHO] **T5** isomerization is a two-step process and goes through a triplet intermediate **T4**, which lies about 1−2 kcal/mol below the initial reactants (see Scheme 1). The formation of **T4** from the initial adduct •C_6H_6O• **T1** is not competitive even under combustion conditions, as it proceeds through a ring-closure **TS4** facing a very high barrier of 32.3 kcal/mol, about 22 kcal/mol higher than that for the dominant **T1** → **TS2** → c-C_6H_5O• + H• pathway. As such, the subsequent chemistry of **T4** (see Scheme 1) leading ultimately to decomposition to c-C_5H_5• + •CHO after conversion to **T5**, is irrelevant. Note that no experimental evidence supports the formation of c-C_5H_5• + •CHO.

We will now shortly discuss the remaining reaction pathways depicted in Scheme 1; only the kinetically important pathways are show with their energies in Figure 1. Attack of the oxygen atom onto a C atom in benzene can take place via both **TS1** and **TS1ex** leading to the vibrationally excited •C_6H_6O• adduct biradicals **T1** (^{3}A′ state) and **T1ex** (^{3}A″ state), respectively, facing barrier heights of 4.1 and 4.3 kcal/mol. It is of interest to note that **TS1** is slightly earlier than **TS1ex**, i.e. the C−O bond distance of 1.917 Å in **TS1** is slightly longer than that of 1.884 Å in **TS1ex** (see Figure 2). As **TS1** and **TS1ex** determine the initial addition rate coefficient, we carried out IRCMax-(CBS-QB3:B3LYP)[64] calculations to obtain more precise energies, generating the values of 4.7 and 4.8 kcal/mol, respectively. These values are in excellent agreement with the experimental Arrhenius activation energy of ca. 4−5 kcal/mol.[15,22,24−29] **T1** and **T1ex**, both belonging to the C_s point group but having distinct electronic states, lie −14.5 and −9.3 kcal/mol below the initial reactants, respectively. Note that optimization of •C_6H_6O• without imposing a C_s symmetry always converged to **T1**. The two highest, singly occupied molecular orbitals (SOMOs), depicted in Figure 4, are the key to the difference between **T1** and **T1ex**. Both SOMOs of **T1** have an A′ symmetry, resulting in a ^{3}A′ electronic state for **T1**. While the first SOMO is formed by a combination of four π orbitals located at four different atom centers, the second SOMO mainly concentrates at the O atom. In contrast, the two SOMOs of **T1ex** have distinct symmetries, an A′ for the first SOMO and an A″ for the second, resulting in a ^{3}A″ electronic state for **T1ex**. While the first SOMO is completely located at the O atom center and

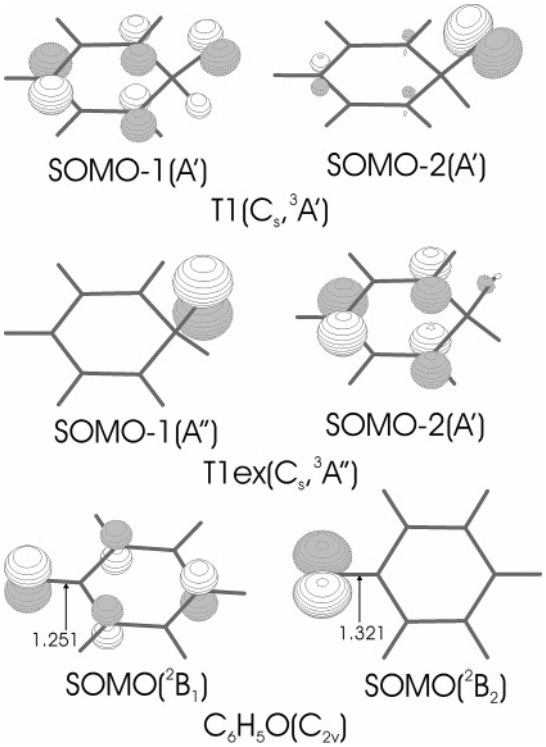

Figure 4. Highest singly occupied molecular orbitals (SOMO) for the two key triplet $^{\bullet}C_6H_6O^{\bullet}$ adducts and the product phenoxy radical.

is perpendicular to the molecular symmetry plane, the second is generated by a combination of three different π orbitals.

T1ex, once formed, either can preferably redissociate back to the initial reactants via **TS1ex** with a low barrier height of 13.6 kcal/mol or could decompose by a H-elimination via **TS2ex** leading to excited products c-$C_6H_5O^{\bullet}(A^2B_2)$ + $H^{\bullet}$, facing a higher barrier of 25.8 kcal/mol, or third could carry out an nonradiative internal conversion (IC) process to **T1**, the lowest-lying triplet adduct. Clearly, the second pathway cannot compete with the first. Hence, the fate of **T1ex** is expected to depend mainly on its rate of redissociation and on the IC rate. Our RRKM rate coefficients for redissociation averaged over the internal energy distributions, as a function of temperature, showed that this rate sharply increases with temperature, i.e., from 1.7×10^8 s^{-1} at 300 K through 8.6×10^{10} s^{-1} at 1000 K to 1.2×10^{12} s^{-1} at 2000 K (see Figure S16 in the Supporting Information). Lack of accurate dynamic calculations prohibited us from gaining an accurate IC rate, which can only be estimated to be roughly 10^{11} s^{-1}.[65,66] Therefore, it is reasonable to conclude that redissociation likely predominates at high temperatures ($T \geq 1500$ K), whereas the IC is likely to be faster at low temperatures ($T \leq 800$ K). In the intermediate range, 800 K < T < 1500 K, these two routes are competitive.

The lowest-lying triplet $^{\bullet}C_6H_6O^{\bullet}$ adduct **T1** can either undergo H-elimination via **TS2** to yield ground state product radicals phenoxy + H, facing a low barrier height of 10.5 kcal/mol, or it can redissociate back via **TS1** to the initial reactants, after clearing a higher barrier of 18.6 kcal/mol. As **TS2** is furthermore looser than **TS1**, this should result in the dominance of the H-elimination step. A third pathway of triplet **T1** is nonradiative transition to the singlet biradical $^{\bullet}C_6H_6O^{\bullet}$ **S1**, followed by isomerization of **S1** to singlet phenol and/or benzene oxide (see discussions below). Scheme 1 shows a number of other reaction pathways for **T1** which where not included in Figure 1 as they are all energetically highly unfavorable and were found in the kinetic analysis to be ineffective in the product formation. The lack of importance of the route of **T1** to CHO + cyclopentadienyl via **T4** and **T5** has already been addressed in detail above. An alternative channel is ring-closure of **T1** leading to **T6** via the tight **TS8**, facing a barrier of 14.1 kcal/mol, i.e., higher than that many of the other **T1** pathways above. **T6** could subsequently undergo ring-opening to **T7** after clearing a barrier of 18.8 kcal/mol, but will much more rapidly reisomerize back to **T1**, over a barrier of only 1.9 kcal/mol. As a result, the **T1** → **T6** → **T7** pathway is entirely negligible. **T1** could also undergo a ring-opening via **TS9** giving rise to **T8** after overcoming an energy barrier of 22.4 kcal/mol, i.e., 11.9 kcal/mol above that of the **T1** → **TS2** → phenoxy + H channel. In addition, **TS9** is much tighter than **TS2**. Hence, the **T1** → **TS9** → **T8** route and all of its subsequent chemistry plays only a very minor role, estimated to be ~1% of the total chemical reactive flux from **T1** (vide infra), and will therefore not be discussed in detail. The 1,2-H shift of **T1** leading to **T2**, via **TS10**, needs to surmount a huge barrier of 29.2 kcal/mol, and is therefore kinetically irrelevant. The lack of reaction flux through these last two channels also closes a different potential **T5** formation route—and hence c-C_5H_5 + CHO formation from **T5**—through **T3** → **T10** → **T11** → **T9** → **T13** → **T12** → **T5**.

It is of interest to briefly discuss the two lowest-lying electronic states (X^2B_1 and A^2B_2) of the phenoxy radical formed in the reactions described above, as it is common as a key intermediate in aromatic flames.[4,5,67] The ground state X^2B_1 of phenoxy lies 23.1 kcal/mol (ca. 1 eV) lower in energy than the first excited state A^2B_2. The single occupied molecular orbital (SOMO) in the X^2B_1 state is formed by a combination of four π orbitals, located at four different centers and all being perpendicular to the molecular symmetry plane (see Figure 4), while the SOMO in the A^2B_2 state is completely located at the O atom center and lies in the molecular symmetry plane. This results in the C−O bond length of 1.251 Å in the X^2B_1 state being closer to a CO double bond length, whereas the length of 1.321 Å in the A^2B_2 state is closer to a CO single bond. In the O + C_6H_6 reaction, the yield of the excited A^2B_2 state is very small and estimated to be less than 5% of the total amount of phenoxy radical. If the A^2B_2 state is formed, it is expected to rapidly perform an IC process to the X^2B_1 state. In flames, the major phenoxy consumption pathway is well established to be its pyrolysis to yield c-C_5H_5 + CO.[67]

In summary, the O-addition onto a C atom in benzene yields both **T1** and **T1ex**. At low temperatures, **T1ex** preferably undergoes an IC process to **T1**, whereas redissociation of **T1ex** back to the initial reactants is predominant at high temperatures. **T1** will mainly eliminate H to yield the phenoxy radical, which is hence expected as the major product of the O-addition mechanism on the triplet PES, in good agreement with experiments.[12,13]

H-Abstraction by O Atom. The O atom can also attack an H atom in benzene in an H-abstraction mechanism. The attack takes place in the molecular plane of symmetry; the two transition structures **TS3a** and **TS3b** are planar and belong to a C_{2v} point group (see Figure 1), in good agreement with observations on the rotational energy of the OH product in a crossed molecular beam experiment.[16] The H-abstraction can occur on both the $^3B_1$ and $^3B_2$ electronic state surfaces, which directly correlate to hydroxyl radical in its Π electronic state. The pathway on the $^3B_1$ surface goes through **TS3a** representing a barrier of 11.6 kcal/mol and leads to a weak complex $C_6H_5^{\bullet}$ ··HO bound by only 2 kcal/mol relative to the separated phenyl and hydroxyl radicals, and as such readily decomposing to these products. The pathway on the $^3B_2$ electronic state passes over

TS3b to directly yield products c-$C_6H_5^\bullet$ + $^\bullet$OH, after clearing a barrier height of 12.3 kcal/mol, only 0.1 kcal/mol above the products. Therefore, both **TS3a** and **TS3b** are loose and very late, i.e., product-like. Note that the H-abstraction mechanism was earlier characterized by Barckholtz et al.[17] using the B3LYP/6-31G(d) level. However, only the $^3B_1$ channel O + c-C_6H_6 → **TS3a** → c-$C_6H_5^\bullet$ + $^\bullet$OH was considered, giving rise to an underestimation for the H-abstraction rate.

It is of interest to evaluate the role and contribution of the chemical flux for the H-abstraction pathways compared to the O-addition channels. For this purpose, we evaluated the temperature-dependent rate coefficients $k(T)$ for both mechanisms using conventional transition state theory (see eqs 11 and 12 below). Since the O + c-C_6H_6 → c-$C_6H_5^\bullet$ + $^\bullet$OH reaction channel faces a barrier of ca. 12 kcal/mol, it is expected to play a role only at high temperatures. We therefore limit this branching ratio evaluation to the $T = 1000-2000$ K range, where we can further make the assumption that the O-addition route on the $^3A''$ surface is only marginal. The latter route may indeed be neglected safely above 1500 K, where redissociation of **T1ex** should predominate over the IC process (see above), but in the $T = 1000-1500$ K range its neglect should entail some underestimation of the overall O-addition fraction.

$$\text{Fraction}_{\text{H-abs}} = \frac{k(T)_{\text{H-abs}}}{k(T)_{\text{H-abs}} + k(T)^{\text{TS1}}_{\text{O-add}}} \tag{11}$$

$$\text{Fraction}_{\text{O-add}} = \frac{k(T)^{\text{TS1}}_{\text{O-add}}}{k(T)_{\text{H-abs}} + k(T)^{\text{TS1}}_{\text{O-add}}} \tag{12}$$

with

$$k(T)_{\text{H-abs}} = \frac{k_b T}{h} \times \frac{\kappa_{\text{TS3a}} \times Q^{\neq}_{\text{TS3a}} \times \exp(-E^{\neq}_{\text{TS3a}}/RT) + \kappa_{\text{TS3b}} \times Q^{\neq}_{\text{TS3b}} \times \exp(-E^{\neq}_{\text{TS3b}}/RT)}{Q_{\text{O}} Q_{\text{C}_6\text{H}_6}} \tag{13}$$

and

$$k(T)^{\text{TS1}}_{\text{O-add}} = \frac{k_b T}{h} \times \frac{Q^{\neq}_{\text{TS1}} \exp(-E^{\neq}_{\text{TS1}}/RT)}{Q_{\text{O}} Q_{\text{C}_6\text{H}_6}} \tag{14}$$

where Q_X is the complete partition function of the given X, including the rotational symmetry number, k_b is Boltzmann's constant, h is Planck's constant, R is the universal gas constant, $E^{\neq}_{TS}$ is the energy of transition structure TS relative to the initial reactants, and κ_{TS} is the one-dimensional tunneling correction for H-abstraction, which is computed by assuming an asymmetric Eckart potential.[68,69] The reaction pathway degeneracy is derived from the symmetry numbers in the partition function for rotation and is equal to 12 for the O-addition and 6 for two H-abstraction channels. This is obvious for the H-abstraction (6 hydrogens) with transition structures being planar and also easy to see for the addition to C atoms: there are six of these carbons, and attack can come from two sides, exactly equivalent for each of the lobes of the π-bond.

The computed results presented in Figure 5 show that the fraction of the H-abstraction flux depends strongly on temperatures, i.e., ~8% at 1000 K and ~32% at 1500 K, which rises to ~53% at 2000 K, indicating that the H-abstraction reaction channels contribute in a major way at combustion temperatures. It should be repeated here that the $^\bullet$OH product in the O + C_6H_6 reaction was observed in the crossed molecular beam experiment at a high collisional energy of 16.5 kcal/mol,[16] but could not be detected earlier in thermal experiments at $T <$ 1500 K.[13,15,22] In contrast, the fraction of the O-addition flux almost linearly decreases with increasing temperatures, from ~92% at 1000 K to ~47% at 2000 K. These results can explain the over-prediction of the phenoxy radical yield in kinetic modeling studies of C_6H_6/O_2 flames because the H-abstraction pathway was not taken into account.[14]

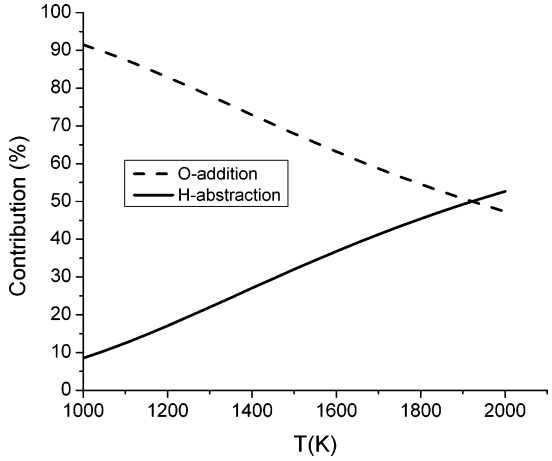

Figure 5. Multistate TST-computed contributions of the H-abstraction and O-addition fluxes as a function of temperature in the $T = 1000-2000$ K range.

The Lowest-Lying Singlet Surface. As mentioned above, almost all experimental studies[12,18-21] show singlet phenol to be one of most important products for the title reaction. In addition, benzene oxide was experimentally detected earlier[18] and very recently cyclohexadienone, butadienyl ketene, and benzene oxide have been observed in an argon matrix study.[23] Moreover, the product CO was found by some groups.[19,21] All these products must be formed on a singlet PES, reached via a spin-forbidden mechanism starting from the initial triplet $^\bullet C_6H_6O^\bullet$ adduct. Hence, the title reaction must also involve the (lowest-lying) singlet surface following an intersystem crossing (ISC) process.

Our RRKM calculations of the decomposition rate of the chemically activated triplet $^\bullet C_6H_6O^\bullet$ **T1** via the two channels **T1** → **TS1** → O + C_6H_6 and **T1** → **TS2** → c-$C_6H_5O^\bullet$ + $^\bullet$H (see Figure 1) show that the summed $\langle k(E)\rangle$ averaged over the nascent energy distribution increases sharply with temperature, i.e., ~10^{10} s^{-1} at 300 K, through ~3.5×10^{11} s^{-1} at 1000 K, and to ~3×10^{12} s^{-1} at 2000 K (see Figure S17 in the Supporting Information). So, the lifetime of **T1** is very short, especially at higher temperatures; i.e. ~100 ps at 300 K, ~3 ps at 1000 K, and down to ~0.35 ps at 2000 K. Therefore, the triplet-to-singlet intersystem crossing of $^\bullet C_6H_6O^\bullet$ is only expected to occur at low to moderate temperatures ($T <$ 1000 K) since the ISC rate can be estimated to be ca. 10^{10} s^{-1}.[65,66] In addition, a (near-)crossing region of the triplet and singlet surfaces is expected to occur in the vicinity of the equilibrium geometry of triplet $^\bullet C_6H_6O^\bullet$ **T1**, since a small triplet-singlet energy gap of 2.7 kcal/mol was obtained at the CASPT2//CASSCF level and spin−orbit coupling is small for first-row elements. Thus, at low temperatures where the decomposition lifetime of **T1** is ~100 ps, the chemically activated, vibrating **T1** adduct can access the crossing region many times, resulting in an increased transition probability and ISC rate.

Because there are 33 degrees of freedom for C_6H_6O species, it is prohibitive to characterize the entire crossing seam between

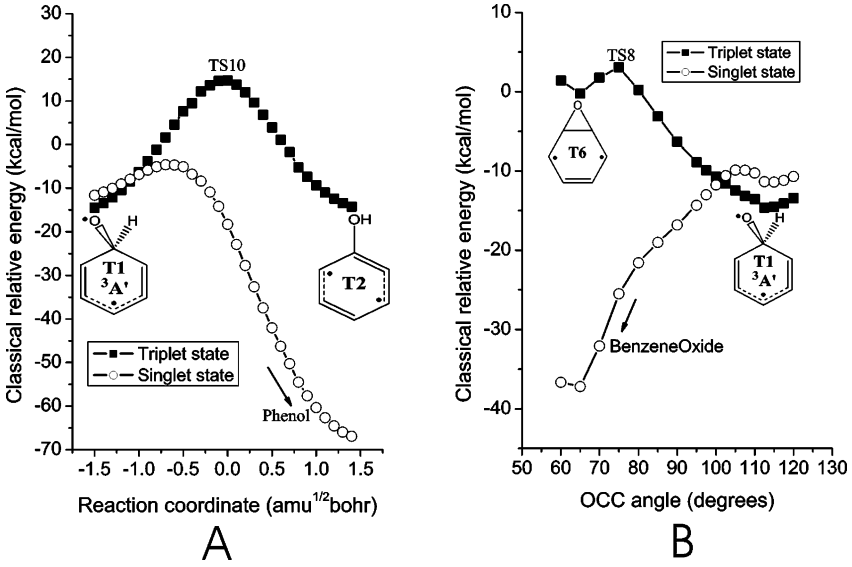

Figure 6. Crossing seams between triplet and singlet surfaces: (A) leading to singlet phenol; (B) yielding singlet benzene oxide.

the two electronic states, ^{3}A′ and ^{1}A′, of oxybenzene. One could restrict the search for a crossing region by determining which modes would promote the nonradiative ^{3}A′ → ^{1}A′ transition in oxybenzene. Such dynamic calculations would be very helpful, but are beyond the scope of this paper.

For the singlet •C$_6$H$_6$O• species, we characterized two forms, **S1** and **S1ex**, with different electronic states, ^{1}A′ and ^{1}A″, respectively; their geometries differ mainly in C−O bond length and C−C−O angle (see Figure S58 in the Supporting Information). **S1** and **S1ex** lie 2.7 and 5.1 kcal/mol higher in energy, respectively, than triplet •C$_6$H$_6$O• **T1**, as computed at the CASPT2/CASSCF level. We thus find that singlet **S1** lies slightly higher than its triplet counterpart **T1**, whereas singlet phenol (**S2**) and singlet benzene oxide (**S6**) lie much lower that their triplet counterparts **T2** and **T6**. Therefore, it can be expected that there are intersections between the triplet and singlet potential energy curves along these two reaction pathways, namely: **T1** → **TS10** → **T2** intersecting with **S1** → **S2**; and **T1** → **TS8** → **T6** intersecting with **S1** → **S6**. We therefore used triplet UB3LYP optimized geometries along two IRC routes, **T1** → **TS10** → **T2** and **T1** → **TS8** → **T6**, to compute energies of the triplet and singlet wavefunctions at the CASPT2(8,8)/cc-pVDZ level, also allowing us to examine the vertical energy difference between the triplet and singlet surfaces. The results are presented in Figure 6, parts A and B, for phenol and benzene oxide, respectively. These figures show that the crossing regions are very close to the harmonic vibrational regions of triplet •C$_6$H$_6$O• **T1**. As shown in Figure 6, two crossing points were located, each about 5 kcal/mol above **T1**, one intersecting the singlet surface directly connecting to phenol, the other to benzene oxide. The intersection leading to phenol appears much more prone to result in actual ISC, as the triplet and singlet surfaces are much closer to one another over a larger RC range than for the intersection yielding benzene oxide. It should be mentioned that in crossed molecular beam experiment the ISC process was found to speed up when the collision energy increased from 2.5 to 6.5 kcal/mol,[12] suggesting that crossing is facilitated by activation of the triplet adduct **T1**.

In any case, once formed from the initial triplet adduct **T1** by ISC, the chemically activated singlet oxybenzene will rapidly rearrange either to singlet phenol by 1,2-H migration or to singlet benzene oxide by ring closure. The various reaction pathways starting at singlet phenol or benzene oxide are schematically presented in Scheme 2, and the most important channels are depicted in Figures 7 and 8. During the course of this work, an article of Xu and Lin[70] was published, presenting ab initio-based kinetics for the unimolecular reaction c-C$_6$H$_5$OH → CO + c-C$_5$H$_6$. Various reaction routes on the singlet PES starting at singlet phenol were theoretically characterized at the G2 M level and discussed in detail by these authors. Our CBS-QB3 values are in good agreement with the G2 M results, generally within 2−3 kcal/mol (see Table S2 in the Supporting Information), similar to the energy differences found in our previous studies.[61,62,71] Therefore, we would like to refer to the work of Xu and Lin[70] for an extensive discussion of the singlet PES, and only summarize that the most favorable reaction routes where found to be: **S2** → **S3** → **S10** → **S9** → CO + c-C$_5$H$_6$ and **S6**/**S7** → **S3** → **S10** → **S9** → CO + c-C$_5$H$_6$. Under low-pressure conditions, the product cyclopentadiene together with CO is theoretically predicted to be always major, whereas other products such as H$_2$O + c-C$_6$H$_4$ or c-C$_6$H$_5$O• + •H all appear to be minor. However, at moderate to high pressures the chemically activated singlet phenol and/or singlet benzene oxide/oxepin will be thermally stabilized rapidly by deactivating collisions with the bath gas. As a result, under these conditions singlet phenol and/or singlet benzene oxide/oxepin are the major products formed on the singlet PES.

III.2. Quantification of the Product Distribution Resulting from O-Addition. The overall contributions of the independent O-addition and H-abstraction channels, as a function of temperature, have already been discussed (see, e.g., Figure 5). In this section, we will first discuss the product distributions resulting from O-addition, as predicted for the separate triplet and singlet surfaces, considered as adiabatic.

On the Triplet PES. As already mentioned above, there are two lowest-lying triplet surfaces (i.e., ^{3}A″ and ^{3}A′, see Figure 1). For the ^{3}A″ surface, redissociation back to the initial reactants is the predominant fate at high temperatures ($T \geq 1500$ K), whereas internal conversion (IC) of **T1ex** to **T1** prevails at low temperatures ($T \leq 500$K). At intermediate temperatures, redissociation and IC both contribute and compete with each other, such that the product distribution on this ^{3}A″ surface strongly depends on the IC rate, which can be obtained only by very demanding dynamic calculations that are beyond the scope of this paper. Therefore, in a first approximation, we assumed that

SCHEME 2: Various Reaction Pathways for the O + C_6H_6 Reaction on the Lowest-Lying Singlet PES Starting at Phenol or Benzene Oxide, Which Are Formed by an ISC Process from the Initial Triplet PES to the Singlet PES, Where Bold Arrows Indicate Dominant Reaction Routes

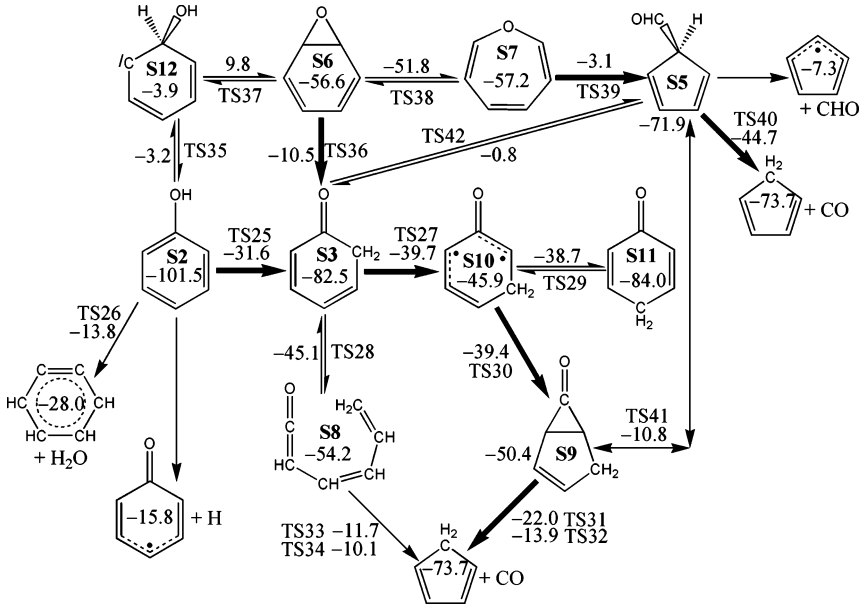

T1ex either completely redissociates back to the reactants or goes entirely toward **T1**, which subsequently proceeds along various reaction pathways on the $^3A'$ surface. The consequences of this assumption and how it could affect the overall thermal rate coefficients will be discussed in section III.3.

The product formation on the $^3A'$ surface will first be discussed without yet accounting for the fraction of ISC fraction of **T1** toward singlet phenol or benzene oxide. There are only three channels of any importance occurring on the $^3A'$ surface: redissociation back into the reactants, production of c-$C_6H_5O^\bullet$ + $^\bullet$H, and collisional stabilization of the initial adduct **T1**. The yields of these three product channels, as a function of temperature and pressure (T = 300−2000 K; $P = 10^{-1}-10^5$ Torr), have been obtained by solving the weak-collision master equation and are presented in Figure 9. As can be seen, the fraction of redissociation back to the initial reactants increases with temperature, but is almost pressure-independent. However, the redissociation route remains minor even at T = 2000 K with a yield <10%. The most important product is c-$C_6H_5O^\bullet$ + $^\bullet$H, which actually makes up close to 100% of all final products over wide T and P ranges. It is only at low temperatures (≤500 K) combined with very high pressure (≥100 atm) that collisional stabilization of the initial oxybenzene adduct **T1** becomes important also as a product route, increasing monotonously with increasing pressure. Actually, under all relevant conditions of hydrocarbon combustion, phenoxy radical + H is the quasi-unique O-addition product formed on the triplet surface, whereas the yield of stabilized **T1** is negligible, < 1% even at T = 1500 K and $P = 10^5$ Torr. This result is a consequence of the very short lifetime of the nascent chemically activated **T1** adduct (<1 ps at T = 1500 K), given also that it requires many collisions to bring its energy below the lowest-lying decomposition transition structure, **TS2**. Any thermally stabilized triplet oxybenzene **T1** is predicted to then undergo the ISC step to the singlet surface, followed by either ring-closure to lead to singlet benzene oxide/oxepin or a 1,2-H shift to yield singlet phenol. It is worth stressing here that the nascent, vibrationally excited triplet oxybenzene can also undergo a same ISC process leading to singlet phenol or benzene oxide, in competition with its

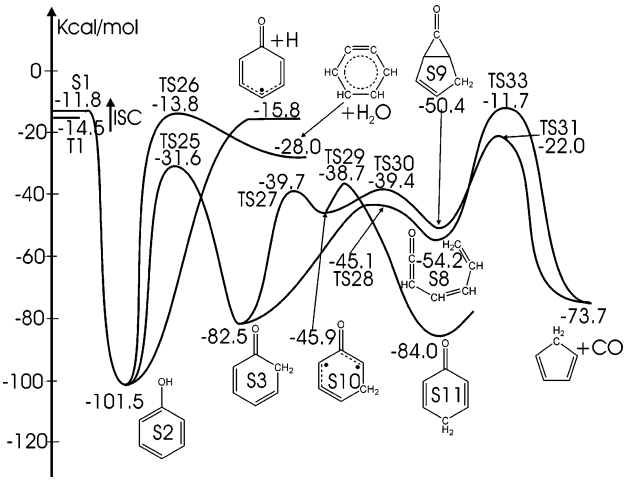

Figure 7. Part of the lowest-lying singlet PES starting at singlet phenol, as computed at the CBS-QB3 level of theory. The arrow indicates ISC crossing from the initial triplet to singlet surfaces.

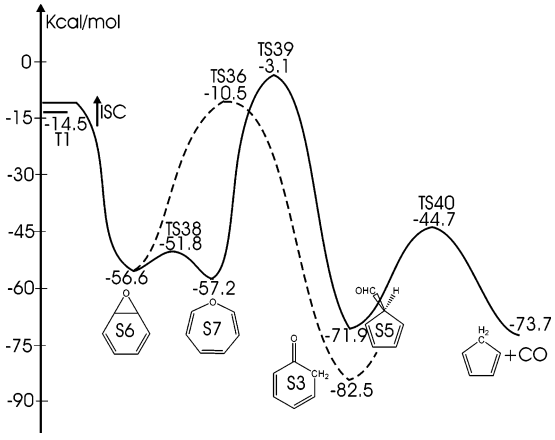

Figure 8. Part of the lowest-lying singlet PES starting at singlet benzene oxide, as computed at the CBS-QB3 level of theory. The arrow indicates ISC crossing from the initial triplet to singlet surfaces. Dashed lines present a connection from singlet benzene oxide to singlet 2,4-cyclohexadienone (**S3**) in Figure 7.

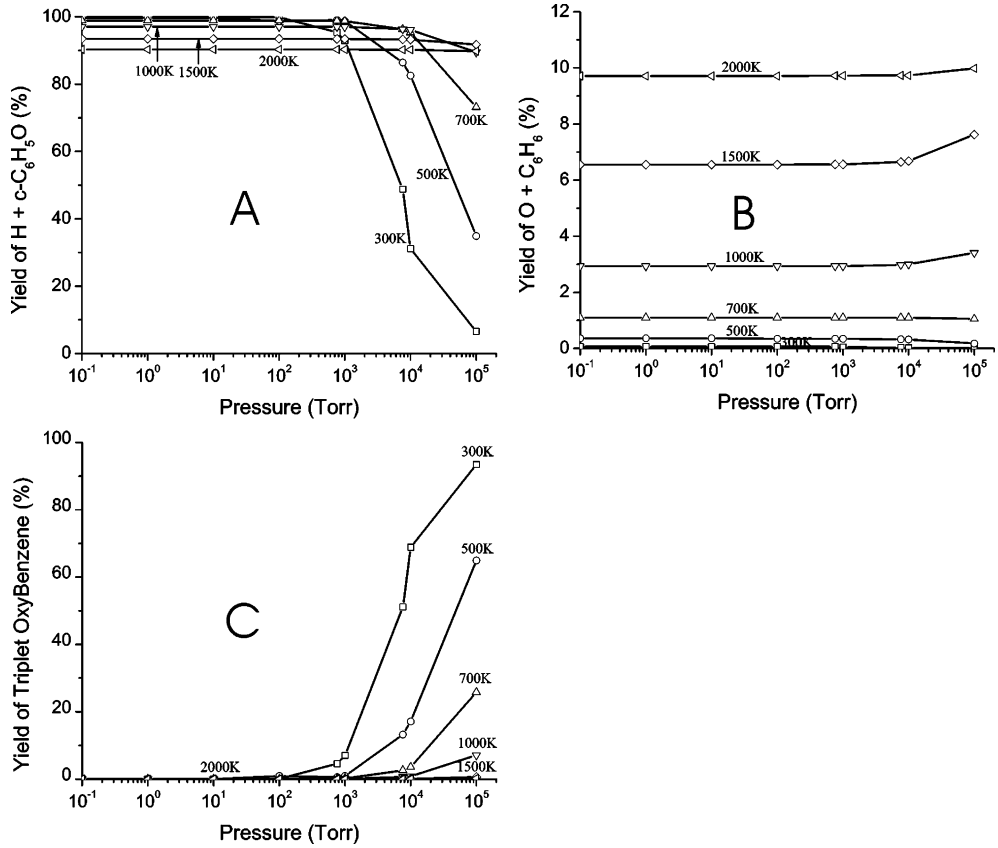

Figure 9. Product distribution on the triplet PES as a function of temperature and pressure: (A) for H• + c-C_6H_5O•; (B) for O + C_6H_6; (C) for collisional stabilization of triplet oxybenzene.

chemically activated fragmentation on the triplet surface, leading to phenoxy + H.

On the Singlet PES. Singlet phenol and benzene oxide when formed from triplet oxybenzene by ISC will undergo subsequent isomerization/decomposition steps or collisional stabilization. The product distribution on the singlet surface is of course dependent on the ratio of the initial singlet phenol and benzene oxide formation, i.e., the ratio of the ISC rates from triplet oxybenzene to singlet phenol and benzene oxide, respectively. Again, ISC rate calculations are beyond our capabilities. Therefore, calculations of the product distribution on the singlet surface were carried out for two extreme cases: the first for the ISC of **T1** yielding only singlet phenol and the second for this process giving only singlet benzene oxide. Note however that the entire singlet PES is included in the master equation analyses; i.e., both regions shown in Figures 7 and 8 are included in the kinetic reaction scheme at all times. It is worth stressing here that, as a result, products distributions for any intermediate case, i.e., initial fractions f of phenol and $1 - f$ of benzene oxide, will simply be the correspondingly weighted sum of the product distributions for the two extreme cases. A number of other important points should also be mentioned here first. (i) Since the c-$C_6H_5OH \rightarrow$ c-C_6H_5O• + •H channel is barrierless, we characterized the kinetic bottleneck structure using variational transition state theory. The variational TS thus located has a O−H bond length of 2.0 Å at an internal energy of 6.5 kcal/mol above the reactants (see Figure S18 in the Supporting Information); the rovibrational parameters of this TS will be used in subsequent product distribution analyses. (ii) The benzene oxide (**S6**) ↔ oxepin (**S7**) internal rearrangement appears to occur very fast, quickly achieving a microcanonical equilibrium before decomposition can take place, such that their effective density of states is taken as the sum of the two individual densities. (iii) Ring-opening of 2,4-cyclohexadienone (**S3**) leads to butadienyl ketene (**S8**, denoted as BDK) (see Figure 7), which by rapid internal rotation around the C−C axis gives rise to various rotamers. We characterized in total eight different rotamers, four of *Z* (cis) configuration and four of *E* (trans) configuration, according to the orientation of the molecule about the central C═C bond (see Table 1), in agreement with previous findings.[23] However, only *Z*-configurations can readily be generated by the internal rotation around the C−C bond starting at **S8a** in a cis-form, whereas it requires some 60 kcal/mol to break the central C═C π-bond and so form an *E*-configuration. At high temperatures, **S8** may contain sufficient initial energy for this (see Figure 7), but other processes are energetically much more favorable and much faster. On the other hand, rates of internal rotation about the C−C bond of BDK-Z are much faster than those of the ring-closure or decay steps (see Figure S19 in the Supporting Information). Thus, it is entirely justified to treat the density of states for the BDK **S8** intermediate as the sum of the individual densities of the four *Z* configurations. Note that each BDK structure without symmetry (C_1) has a mirror configuration, the density of states of which was also included.

Yields of various product channels computed as a function of $T = 300-2000$ K and $P = 10^{-4}-10^{5}$ Torr are presented in Figure 10 for 100% singlet phenol initially formed by ISC from triplet oxybenzene; and in Figure 11 for 100% initial singlet benzene oxide. An important observation is that the product distributions predicted for these two extreme cases do not differ overly much, except of course for stabilized phenol and benzene oxide at the highest pressures. Hence, the unknown relative contribution of the two ISC processes will not have a major

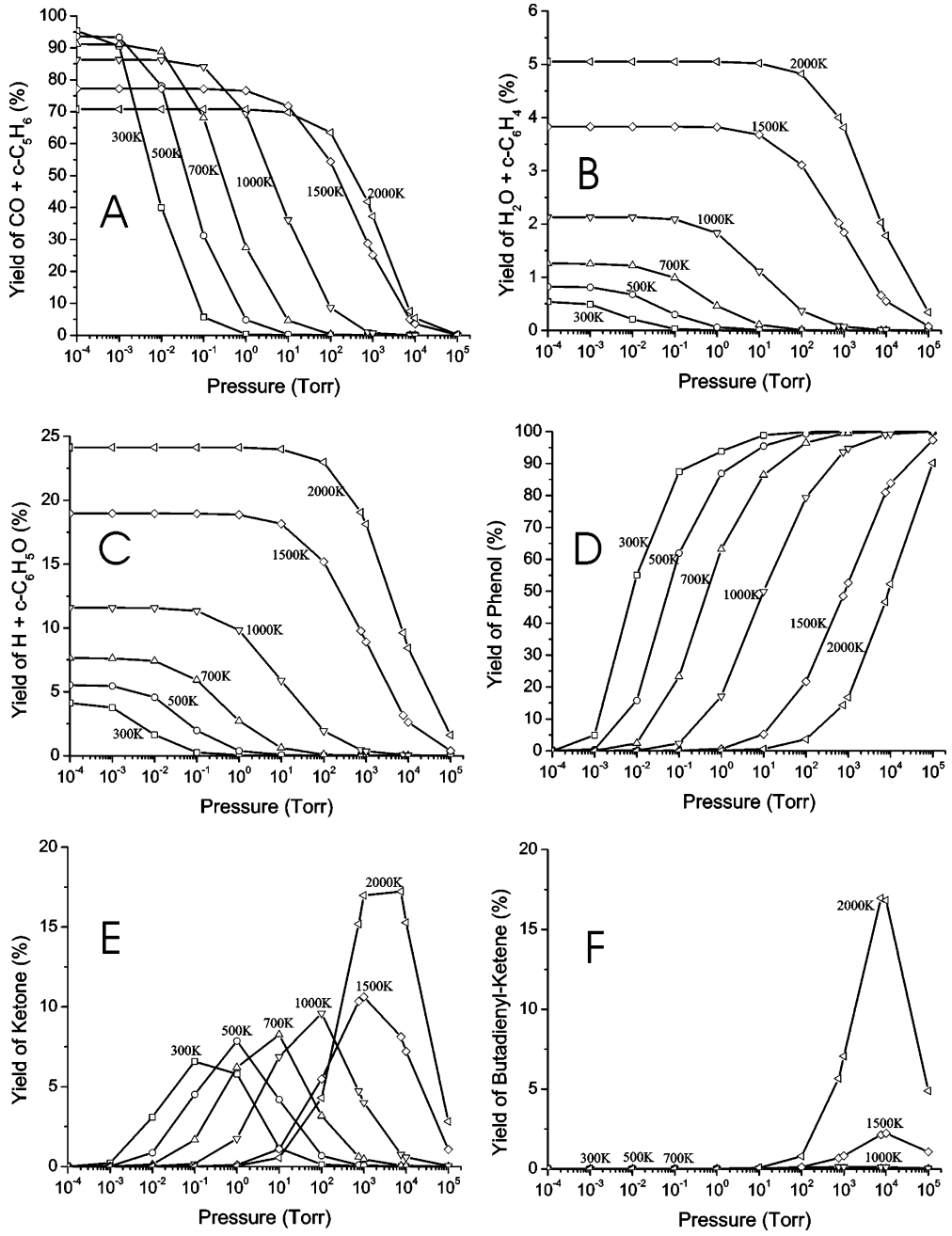

Figure 10. Product distribution on the singlet PES as a function of temperature and pressure, assuming that singlet phenol is the only initial singlet intermediate resulting from ISC of triplet oxybenzene.

impact on the predicted product distribution over the examined T, P ranges. Figures 10 and 11 also show that the products c-C_5H_6 + CO, phenol, and benzene oxide/oxepin are major, at least in some conditions, while the products phenoxy radical + H, c-C_6H_4 + H_2O, the ketone **S3** and BDK **S8** are always minor. These results are in agreement with earlier experimental observations for key products such as phenol and CO.[19−21] As can be seen, the fractions of the various products depend in a complex way on *T* and *P*. In general, an increase of temperature enhances the yields of c-C_5H_6 + CO, phenoxy radical + H, and c-C_6H_4 + H_2O. On the other hand, increasing the pressure will reduce the yields of c-C_5H_6 + CO, phenoxy radical + H, and c-C_6H_4 + H_2O, but increase those of phenol and benzene oxide/oxepin. These temperature and pressure effects are entirely in keeping with the competition between isomerization/decomposition reactions on one hand, and collisional stabilization on the other.

Comparison of Predictions with Experiment. Let us compare our predicted major products to the experimental observations. First, following O-addition, the route to phenoxy radical + H is found to be the dominant if not the sole product pathway on the triplet PES under all hydrocarbon combustion conditions. The phenoxy product was detected not only in earlier collision-free experiment,[12] but also in recent thermal, multicollision experiments.[13] Second, phenol was established as an important product of the title reaction in several experimental studies,[12,18−21] and recognized to result solely from spin-forbidden ISC from the triplet to singlet surfaces. Our present study shows that phenol is preferably generated under low *T* ($\leq$1000 K) conditions where ISC to the singlet surface can more easily outrun the decomposition of the triplet adduct **T1** to phenoxy + H (see further). While formation of phenol in multicollision conditions is easily explained by ISC and collisional stabilization by bath gas molecules/atoms, the

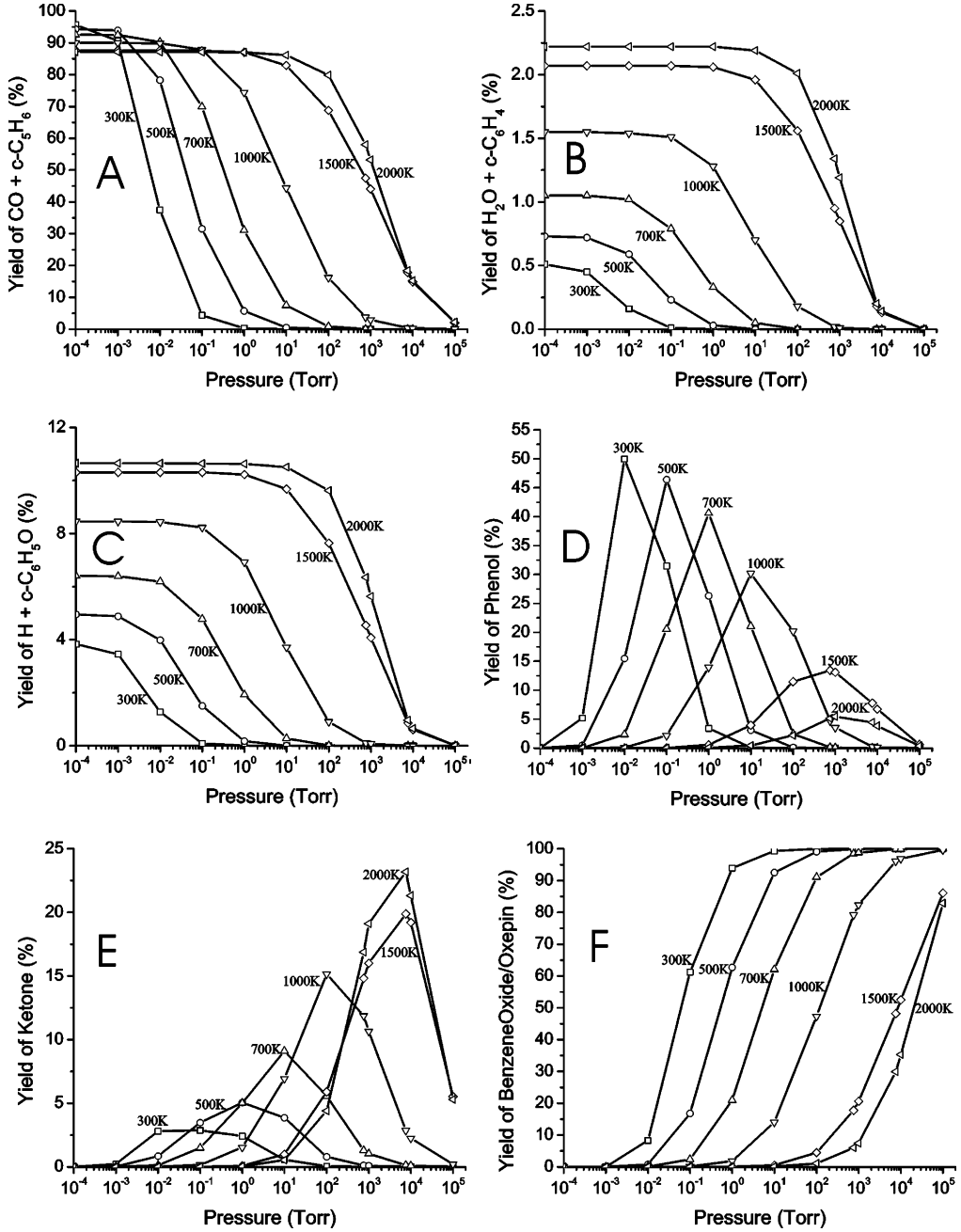

Figure 11. Product distribution on the singlet PES as a function of temperature and pressure, assuming that singlet benzene oxide is the only initial singlet intermediate resulting from ISC of triplet oxybenzene.

observation of phenol in single-collision crossed molecular beam experiments[12] is not understood completely. Lee et al.[12] rationalized their detection of important amounts of phenol at a flight time of 200 μs after the reactive O + C_6H_6 encounter as being due to a long lifetime of the hot singlet c-C_6H_5OH intermediate formed upon ISC. To test this hypothesis, we investigated the time evolution of the abundance of the various intermediate and product species in the O + C_6H_6 reaction, assuming that of the 6.5 kcal/mol collision energy in the mentioned experiment, only the 4.1 kcal/mol required to surmount the addition barrier contributes to the internal energy of the initial adduct and ensuing singlet intermediates, i.e., either phenol or benzene oxide. In this RRKM analysis, the motion of the hydroxyl-H about the O−C axis in phenol was treated as a free internal rotation, quite justifiable at the 105.6 kcal/mol internal energy of the hot phenol at issue. The results, plotted in Figure 12, parts A and B, indicate that after 200 μs much of the initial singlet phenol/benzene oxide should still survive, while most of the remainder should have decayed to CO + c-C_5H_6. Given the abundance changes predicted around 100 μs (see Figure 12), and considering the estimated uncertainties of a factor of 2 or 3 regarding our theoretical RRKM lifetimes of the singlet intermediates, the present results are consistent with the Lee et al. findings and rationalizations,[12] even though their observation that CO is only a minor product after 200 μs suggests an overestimation on our part of the hot phenol/benzene oxide decomposition rate. At the same time, our analysis offers an qualitative explanation why in the crossed-beam experiment of Sloane,[21] at only 0.6 kcal/mol collision energy and hence longer flight times, CO and C_5H_6 were observed as major products, at least on a par with singlet [C_6H_6O] compounds. It may be noted that only the fragmentation products CO + c-C_5H_6 and in a minor way H + phenoxy resulting from the hot singlet [C_6H_6O]

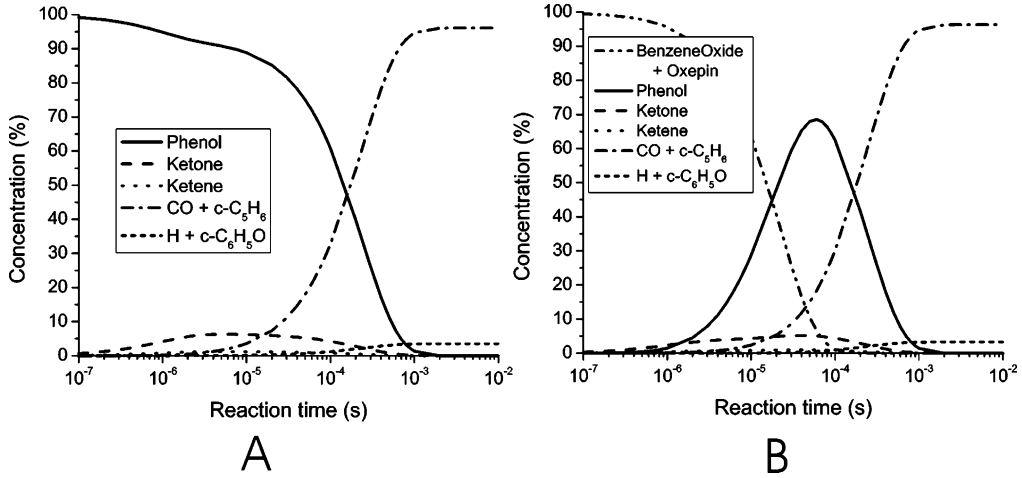

Figure 12. Time-evolution of abundances of species on the lowest-lying singlet surface under single-collision conditions at a total energy equal to the lowest-lying entrance TS, i.e., 4.1 kcal/mol above the reactants (see text). Case A starting at singlet phenol and case B starting at singlet benzene oxide, respectively, as initial activated singlet intermediate.

intermediates should be considered as true singlet-surface "end"-products in single-collision conditions.

Third, in thermal conditions, the product benzene oxide/oxepin is predicted to be produced on the singlet PES at low T and moderate P; it was indeed detected earlier as a transient intermediate[18] in the O + C_6H_6 reaction and also observed in a recent argon matrix study at 12 K.[23] Fourth, H-abstraction pathways on triplet surfaces leading to phenyl plus hydroxyl radicals are theoretically characterized and evaluated to contribute significantly at high temperatures; e.g., at $T = 2000$ K their contribution is predicted to be comparable to that of O-addition. The •OH radical was indeed detected in crossed molecular beam experiments at a high collision energy of 16.5 kcal/mol.[16] Finally, the production of CO, which should be formed together with c-C_5H_6, has been a subject of some debate. In our present analysis, we resolve this controversy by rationalizing the production of CO as a major end-product in the particular conditions of crossed molecular beam experiments at longer flight times as reported by Sloane,[21] making clear at the same time why in similar but short flight-time experiments such as that of Lee et al.,[12] CO formation is still less important. It should be noted that the two other studies reporting a negligible CO production with yield ≤ 5%, i.e. Nicovich et al.[22] and Bajaj and Fontijn,[13] were both conducted under thermal, multicollision conditions, at $T = 298-950$ K/$P = 100$ Torr and at $T = 405$ K/$P = 3-12$ Torr, respectively. Again, our present investigation clarifies why CO + c-C_5H_6 production in multicollision conditions differs greatly from that in single-collision experiments. Figures 10 and 11 show that the predicted CO yield from the singlet surface is <10% in T and P ranges of both the above-mentioned thermal experiments.[13,22] If we roughly assume that 50% of the reactive flux goes through ISC, the overall CO yield is estimated to be <5%, in agreement with the experimental findings.[13,22]

A quantitative prediction of the overall product branching ratios spanning all potential energy surfaces is at this time difficult due to the need for accurate dynamic calculation on the rates of the IC and ISC processes involved. For these systems such calculations are extremely demanding and beyond our current computational resources. An alternative approach, used successfully in earlier work,[61,62] where the ratio of ISC crossing vs on-surface unimolecular reactions is calibrated against experimental product measurements, is not possible here due to the current lack of sufficiently complete experimental product distribution data.

III.3. Overall Thermal Rate Coefficient. The overall temperature-dependent rate coefficient $k(T)_{overall}$ for the O(^{3}P) + C_6H_6 reaction can be computed according to

$$k(T)_{overall} = k(T)_{O-add} + k(T)_{H-abs} \quad (15)$$

where the $k(T)$ in the right-hand-side (RHS) are the rate coefficient derived from multistate transition state theory:

$$k(T)_{O-add} = (1 - \gamma^{re}_{TS1}) \times k(T)^{TS1}_{O-add} + (1 - \gamma^{re}_{TS1ex}) \times k(T)^{TS1ex}_{O-add} \quad (16)$$

with

$$k(T)^{TS1ex}_{O-add} = \frac{k_b T}{h} \times \frac{Q^{\neq}_{TS1ex} \exp(-E^{\neq}_{TS1ex}/RT)}{Q_O Q_{C_6H_6}} \quad (17)$$

$k(T)^{TS1}_{O-add}$ and $k(T)_{H-abs}$ already defined in eqs 14 and 13 above, respectively, and γ^{re} is the fraction of redissociation of the initial adducts back to the initial reactants, as a function of temperature and pressure (for example, see Figure 9B). At low temperatures ($T \leq 800$ K), redissociation is minor if not negligible and the value of γ^{re} is close to 0. Above 1000 K, redissociation becomes non-negligible, but its contribution is the result of a complicated competition between redissociation, further isomerization, and IC/ISC processes (IC for **T1ex)**. Accurate quantification of γ^{re} therefore again requires dynamic calculations that are beyond our capabilities. We therefore limited ourselves to the calculation of $k(T)_{overall}$ for $T \leq 800$ K; furthermore, for these lower temperatures experimental data are well established and available for comparison. The rotational symmetries for C_6H_6, the O-addition, and H-abstraction transition states are 12, 1, and 2, respectively, such that the reaction path degeneracy is 12 for each O-addition channel, but 6 for each H-abstraction channel as already discussed earlier. The electronic partition function of the O atom explicitly includes the three lowest-lying electronic states ($^3P_2$ with electronic degeneracy $g = 5$, $^3P_1$ with $g = 3$, and $^3P_0$ with $g = 1$), with relative energies of 0.0000, 0.4525, and 0.6490 kcal/mol, respectively.[72] Also, the electronic degeneracy of 3 for the transition structures, having a triplet electronic state, is duly taken into account.

The rate predictions are plotted in Figure 13 and can be well-represented by a modified Arrhenius equation $k(T)_{overall} = 3.7$

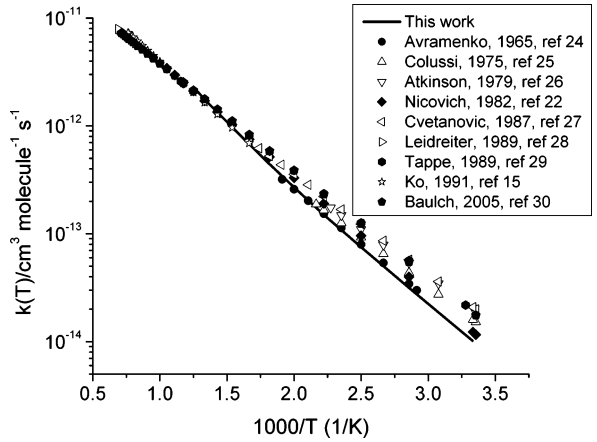

Figure 13. Overall thermal rate coefficient $k(T)$ for the O + C_6H_6 reaction as a function of temperature in the $T = 300-800$ K range, computed using multistate TST theory. The most recent experimental data are presented for the purpose of comparison.

$\times 10^{-16} \times T^{1.66} \times \exp(-1830\ \mathrm{K}/T)$ cm^3 molecule^{-1} s^{-1}; recent experimental data are also shown for comparison. Our $k(T)$ results are in near-perfect agreement with the experimental data of Nicovich et al.[22] and Avramenko et al.[24] over the entire range 300 to 800 K, while they are slightly below the measurements by other authors at low temperatures. At room temperature, our predicted rate coefficient is 1.0×10^{-14} cm^3 molecule^{-1} s^{-1}, in good agreement with the 1.2×10^{-14} cm^3 molecule^{-1} s^{-1} measurement by Nicovich[22] but ca. 40% below the 1.7×10^{-14} cm^3 molecule^{-1} s^{-1} recommended in the literature.[30] However, at higher temperatures, the agreement with experimental data improves considerably. It should be noted that our CBS-QB3 computed barrier heights prove to be reliable and within "chemical accuracy", given that 0.5 kcal/mol difference alters the computed $k(T)$ values at room temperature by a factor of 2.3.

IV. Concluding Remarks

In the present theoretical study, the lowest-lying triplet and singlet potential energy surfaces for the O(^{3}P) + C_6H_6 reaction were characterized, uniformly using the high level quantum chemical CBS-QB3 method. RRKM master equation calculations to evaluate primary product distribution for each of these surfaces separately and to qualitatively predict the overall major products were carried out using the exact stochastic simulation method. In addition, overall thermal rate coefficients were determined in the 300−800 K range using multistate transition state theory. A number of important results emerge from this study and can be summarized as follows:

(i) The O(^{3}P) + C_6H_6 reaction is confirmed to occur mainly, but not exclusively, via an electrophilic O-addition mechanism as the first reaction step. The predicted major products from this addition reaction are c-$C_6H_5O^\bullet$ + $H^\bullet$ together with phenol and/or benzene oxide/oxepin. c-$C_6H_5O^\bullet$ + $H^\bullet$ are the most important products in flame conditions and nearly exclusively formed on the lowest-triplet PES, whereas phenol and/or benzene oxide/oxepin are mainly produced from the lowest-lying singlet surface following an ISC process; these results confirm the available experimental observations. CO + c-C_5H_6 are predicted to be formed in flames, but with yields that can be important only around atmospheric pressure or below. In single-collision crossed molecular beam experiments,[21] CO + c-C_5H_6 should be major end-products at long enough flight times, resulting from the decomposition of chemically activated singlet phenol/benzene oxide formed after ISC. Ketones should be produced as minor products under moderate T and P conditions. The O + C_6H_6 → c-$C_5H_5^\bullet$ + $^\bullet$CHO channel is predicted to be unimportant under all relevant combustion conditions, in contrast with previous theoretical conclusions.[14]

(ii) Separate from O-addition, H-abstraction by O proceeds on two electronic surfaces, $^3B_1$ and $^3B_2$, and results in OH-($X^2\Pi$) + c-$C_6H_5^\bullet$ products, predicted to be major at high temperatures. The contribution of H-abstraction to the overall product formation is estimated to be ca. 50% at 2000 K. Further experimental studies are awaited to validate these predictions.

(iii) The entrance barrier heights and reaction enthalpies computed at the CBS-QB3 level of theory are in good agreement with available experimental data, within 0.5 kcal/mol.

(iv) The lack of accurate dynamic calculations for ISC and IC rates and/or of available experimental product branching ratios prohibits us from quantitatively predicting the overall primary product distribution for the title reaction. However, the present study elucidates the detailed reaction mechanism and semiquantitatively predicts all products, as observed in widely different reaction conditions.

(v) The multistate TST computed overall rate coefficient for this complex multichannel reaction, over the range 300−800 K—$k(T) = 3.7 \times 10^{-16} \times T^{1.66} \times \exp(-1830\ \mathrm{K}/T)$ cm^3 molecule^{-1} s^{-1}—is in good agreement with the experimental data in the literature, within a factor of <2.

Acknowledgment. The authors are indebted to the FWO−Vlaanderen and the KULeuven Research Council (BOF fund) for continuing financial support. T.L.N. and L.V. thank the KULeuven Research Council for a PhD-scholarship and a postdoctoral mandate, respectively.

Supporting Information Available: Table of optimized geometries, zero-point energies, rotational constants, and harmonic vibrational frequencies, and figures showing various graphs of IRC calculations. This material is available free of charge via the Internet at http://pubs.acs.org.

References and Notes

(1) Glassman, I. *Combustion*, 2nd ed.; Academic Press: Boca Raton, FL, 1987.
(2) Gardiner, W. C., Jr. *Combustion Chemistry*; Springer-Verlag: New York, 1984.
(3) Miller, J. A.; Klippenstein, S. J. *J. Phys. Chem. A* **2003**, *107*, 7783.
(4) Richter, H.; Howard, J. B. *Phys. Chem. Chem. Phys.* **2002**, *4*, 2038.
(5) Brezinsky, K. *Prog. Energy Combust. Sci.* **1986**, *12*, 1.
(6) Sawyer, R. F. *Twenty-Fourth Symp. (Int.) Combust.* **1992**, 1423.
(7) Bittner, J. D.; Howard, J. B. *Eighteenth Symp. (Int.) Combust.* **1981**, 1105.
(8) Chai, Y.; Pfefferle, L. D. *Fuel* **1998**, *77*, 313.
(9) Davis, S. G.; Wang, H.; Brezinsky, K.; Law, C. K. *Twenty-Sixth Symp. (Int.) Combust.* **1996**, 1025.
(10) Tan, Y.; Frank, P. *Twenty-Sixth Symp. (Int.) Combust.* **1996**, 677.
(11) From NIST web page: http://srdata.nist.gov/cccbdb/.
(12) Sibener, S. J.; Buss, R. J.; Casavecchia, P.; Hirooka, T.; Lee, Y. T. *J. Chem. Phys.* **1980**, *72*, 4341.
(13) Bajaj, P. N.; Fontijn, A. *Combust. Flame* **1996**, *105*, 239.
(14) Hodgson, D.; Zhang, H. Y.; Nimlos, M. R.; McKinnon, J. T. *J. Phys. Chem. A* **2001**, *105*, 4316 and references therein.
(15) Ko, T.; Adusei, G. Y.; Fontijn, A. *J. Phys. Chem.* **1991**, *95*, 8745.
(16) Barry, N. J.; Fletcher, I. W.; Whitehead, J. C. *J. Phys. Chem.* **1986**, *90*, 4911.
(17) Barckholtz, C.; Barckholtz, T. A.; Hadad, C. M. *J. Phys. Chem. A* **2001**, *105*, 140.
(18) Mani, I.; Sauer, Jr. M. C. *Advan. Chem. Ser.* **1968**, *82*, 142.
(19) Boocock, G.; Cvetanovic, R. J. *J. Can. Chem.* **1961**, *39*, 2436.
(20) Bonanno, R. A.; Kim, P.; Lee, J. H.; Timmons, R. B. *J. Chem. Phys.* **1972**, *57*, 1377 and references therein.
(21) Sloane, T. M. *J. Chem. Phys.* **1977**, *67*, 2267.

(22) Nicovich, J. M.; Gump, C. A.; Ravishankara, A. R. *J. Phys. Chem.* **1982**, *86*, 1684.
(23) Parker, J. K.; Davis, S. R. *J. Am. Chem. Soc.* **1999**, *121*, 4271.
(24) Avramenko, L. I.; Kolesnikova, R. V.; Savinova, G. I. *Bull. Acad. Sci. U.S.S.R. Div. Chem. Sci. (Engl. Transl.)* **1965**, 24−29.
(25) Colussi, A. J.; Singleton, D. L.; Irwin, R. S.; Cvetanovic, R. J. *J. Phys. Chem.* **1975**, *79*, 1900.
(26) Atkinson, R.; Pitts, J. N. *Chem. Phys. Lett.* **1979**, *63*, 485.
(27) Cvetanovic, R. J. *J. Phys. Chem. Ref. Data* **1987**, *16*, 261.
(28) Leidreiter, H. I.; Wagner, H. G. *Z. Phys. Chem.* **1989**, *165*, 1.
(29) Tappe, M.; Schliephake, V.; Wagner, H. G. *Z. Phys. Chem.* **1989**, *162*, 129.
(30) Baulch, D. L.; Cobos, C. J.; Cox, R. A.; Frank, P.; Hayman, G.; Just, Th.; Kerr, J. A.; Murrells, T.; Pilling, M. J.; Troe, J.; Walker, R. W.; Warnatz, J. *J. Phys. Chem. Ref. Data* **2005**, *34*, 854.
(31) Alzueta, M. U.; Glarborg, P.; Dam-Johansen, K. *Int. J. Chem. Kinet.* **2000**, *32*, 498.
(32) Costa, I. D.; Fournet, R.; Billaud, F.; Battin-Lecclerc, F. *Int. J. Chem. Kinet.* **2003**, *35*, 503.
(33) Lindstedt, R. P.; Skevis, G. *Combust. Flame* **1994**, *99*, 551.
(34) Tan, Y.; Frank, P. *Twenty-Sixth Symp. (Int.) Combust.* **1996**, 677.
(35) Becke, A. D. *J. Chem. Phys.* **1993**, *98*, 5648.
(36) Stevens, P. J.; Devlin, F. J.; Chablowski, C. F.; Frisch, M. J. *J. Phys. Chem.* **1994**, *98*, 11623.
(37) Gonzalez, C.; Schlegel, H. B. *J. Chem. Phys.* **1989**, *90*, 2154.
(38) Gonzalez, C.; Schlegel, H. B. *J. Phys. Chem.* **1990**, *94*, 5523.
(39) Montgomery, J. A. Jr.; Frisch, M. J.; Ochterski, J. W.; Petersson, G. A. *J. Chem. Phys.* **1999**, *110*, 2822.
(40) Werner, H. J.; Knowles, P. J. *J. Chem. Phys.* **1985**, *82*, 5053.
(41) Knowles, P. J.; Werner, H. J. *Chem. Phys. Lett.* **1985**, *115*, 259.
(42) Celani, P.; Werner, H. J. *J. Chem. Phys.* **2000**, *112*, 5546.
(43) Frisch, M. J.; Trucks, G. W.; Schlegel, H. B.; et al. Gaussian 03; Gaussian, Inc.: Pittsburgh, PA, 2004.
(44) DALTON, a molecular electronic structure program, written by: Helgaker, T.; Jensen, H. J. Aa.; Joergensen, P.; Olsen, J.; Ruud, K.; Aagren, H.; Auer, A. A.; et al., Release 1.2, 2001.
(45) MOLPRO is a package of ab initio programs written by: Werner, H.-J.; Knowles, P. J.; Schütz M.; Lindh, R.; Celani, P.; Korona, T.; Rauhut, G.; Manby, F. R.; Amos, R. D.; Bernhardsson, A.; Berning, A.; Cooper, D. L.; Deegan, M. J. O.; Dobbyn, A. J.; Eckert, F.; et al. 2002.
(46) Gillespie, D. T. *J. Comput. Phys.* **1976**, *22*, 403.
(47) Gillespie, D. T. *J. Phys. Chem.* **1977**, *81*, 2340.
(48) Gillespie, D. T. *J. Comput. Phys.* **1978**, *28*, 395.
(49) Vereecken, L.; Huyberechts, G.; Peeters, J. *J. Chem. Phys.* **1997**, *106*, 6564.
(50) Matsumoto, M.; Nishimura, T. *ACM. Trans. Model. Comput. Simul.* **1998**, *8*, 3.
(51) Hippler, H.; Troe, J.; Wendelken, H. J. *J. Chem. Phys.* **1983**, *78*, 6709.
(52) Troe, J. *J. Chem. Phys.* **1977**, *66*, 4745.
(53) Forst, W. *Theory of Unimolecular Reactions*; Academic Press: New York, 1973.
(54) Robinson, P.; Holbrook, K. *Unimolecular Reactions*; Wiley-Interscience: London, 1972.
(55) Gilbert, R. G.; Smith, C. S. *Theory of Unimolecular and Recombination Reactions*; Blackwell Scientific: Oxford, U.K., 1990.
(56) Holbrook, K.; Pilling, M.; Robertson, S. *Unimolecular Reactions*, 2nd ed.; Wiley: New York, 1996.
(57) Steinfeld, J. I.; Francisco, J. S.; Hase, W. L. *Chemical Kinetics and Dynamics*; Prentice Hall: Englewood Cliffs, NJ, 1999.
(58) Baer, T.; Hase, W. L. *Unimolecular Reaction Dynamics: Theory and Experiment*; Oxford University Press: Oxford, U.K., 1996.
(59) Beyer, T.; Swinehart, D. F. *Commun. Assoc. Comput. Machines* **1973**, *16*, 379.
(60) Stein, S. E.; Rabinovitch, B. S. *J. Chem. Phys.* **1973**, *58*, 2438.
(61) Nguyen, T. L.; Vereecken, L.; Peeters, J. *J. Phys. Chem. A* **2006**, *110*, 6696.
(62) Nguyen, T. L.; Vereecken, L.; Hou, X. J.; Nguyen, M. T.; Peeters, J. *J. Phys. Chem. A* **2005**, *109*, 7489.
(63) Nguyen, T. L.; Peeters, J.; Vereecken, L. *J. Phys. Chem. A* **2006**, *110*, 12166.
(64) Malick, D. K.; Petersson, G. A.; Montgomery, J. A., Jr. *J. Chem. Phys.* **1998**, *108*, 5704.
(65) Klessinger, M.; Michl, J. *Excited States and Photochemistry of Organic Molecules*; VCH: New York, 1995.
(66) Haas, Y.; Klessinger, M.; Zilberg, S. *Chem. Phys.* **2000**, *259*, 121 and references therein.
(67) Liu, R.; Morokuma, K.; Mebel, A. M.; Lin, M. C. *J. Phys. Chem.* **1996**, *100*, 9314 and references therein.
(68) Eckart, C. *Phys. Rev.* **1930**, *35*, 1303.
(69) Johnston, H. S.; Heicklen, J. *J. Phys. Chem.* **1966**, *66*, 532.
(70) Xu, Z. F.; Lin, M. C. *J. Phys. Chem. A* **2006**, *110*, 1672.
(71) Nguyen, T. L.; Dils, B.; Carl, S. A.; Vereecken, L.; Peeters, J. *J. Phys. Chem. A* **2005**, *109*, 9786.
(72) NIST web page: http://physics.nist.gov/PhysRefData/Handbook/periodictable.htm.
(73) Nguyen, T. L.; Le, T. N.; Mebel, A. M. *J. Phys. Org. Chem.* **2001**, *14*, 131 and references therein.
(74) Wenthold, P. G.; Squires, R. R.; Lineberger, W. C. *J. Am. Chem. Soc.* **1998**, *120*, 5279.
(75) Luo, Y. R. *Handbook of Bond Dissociation Energies in Organic Compounds*; CRC Press: Boca Raton, FL, 2003.